Geochemical Perspectives Letters

Nitrogen isotopic variations in the early Solar System recorded by pallasites

J. Gamblin, E. Füri, B. Luais, L. Zimmermann

Supplementary Information

The Supplementary Information includes:

- Pallasite and Iron Meteorite Samples
- Detailed Methodology
- Correction for the Cosmogenic ^{15}N Contribution
- Tables S-1 to S-5
- Figures S-1 to S-7
- Supplementary Information References

Pallasite and Iron Meteorite Samples

Below is a brief description of each Main Group (PMG), Eagle Station (PES), and ungrouped pallasite analysed in this study. Details of the five IIIAB iron meteorites analysed for comparison are also provided. Pallasites are classified based on the O isotopic compositions of their silicates (Fig. S-1), olivine and metal compositions, and mineralogy. Compared to PMG, PES exhibit lighter O isotopic signatures (Boesenberg *et al.*, 2012; Fig. S–1), higher fayalite contents in their olivines ($Fa_{12\pm1.5}$ for PMG and $Fa_{18.5\pm2}$ for PES; Buseck and Goldstein, 1969), and metal richer in Ni, Ir, and Ge and poorer in Au, As, and Ga (Scott, 1977a). Pyroxene pallasites are classified as "ungrouped" in the Meteoritical Bulletin Database, but their relatively high pyroxene content leads them to be more commonly referred to as "pyroxene pallasites". The metal phases of pallasites and IIIAB iron meteorites are composed of taenite and kamacite—both Fe-Ni alloys, containing up to 7.5 % Ni for kamacite and >25 % Ni for taenite (Buchwald, 1975)—and show bulk Ni contents ranging from 7.8 to 11.7 % in PMG (Scott, 1977a), 14 to 16 % in PES (Scott, 1977a), and 7 to 10.5 % in IIIAB iron meteorites (Krot *et al.*, 2014).

PMG:

PMG have metal compositions closely related to those of evolved IIIAB iron meteorites (Wasson and Choi, 2003), and their olivines display a variety of textures (Scott, 1977b; McKibbin *et al.*, 2019). Some PMG are classified as "anomalous" (PMG-an), either due to their unusual metal compositions (PMG-am, for "anomalous metal") or their high olivine Fa contents (PMG-as for "anomalous silicate"; Wasson and Choi, 2003).

Admire (PMG; Meteoritical Bulletin (MB) 37): has angular and fragmental olivines (McKibbin *et al.*, 2019), locally clustered (Boesenberg *et al.*, 2012), with some variability in their Fe content (Buseck and Goldstein, 1969). Some olivine grains show vermicular troilite intergrowths (Buseck, 1977).

Brahin (PMG; MB 44): exhibits a variety of olivine textures, including angular, rounded, and fragmental grains, with relatively low Mn concentrations (McKibbin *et al.*, 2019).
Esquel (PMG; MB 29): has angular olivines (McKibbin *et al.*, 2019), locally assembled into olivine clusters (Boesenberg *et al.*, 2012).
Fukang (PMG; MB 90): has olivine textures ranging from rounded to angular (< 5 mm to several cm), locally clustered (Boesenberg *et al.*, 2012), with the presence of vermicular troilite intergrowths in some grains (Buseck, 1977). The metal phase consists mainly of kamacite, with taenite present in large metal regions.
Imilac (PMG): has angular and fragmental olivine textures (McKibbin *et al.*, 2019), with rounded microstructures, locally assembled into olivine clusters (Boesenberg *et al.*, 2012).
Seymchan (PMG; MB 43): exhibits a variety of olivine textures, including angular, rounded, and fragmental grains (McKibbin *et al.*, 2019), locally occurring as olivine clusters (Boesenberg *et al.*, 2012).
Brenham (PMG-am): has rounded olivines with relatively low Mn concentrations (McKibbin *et al.*, 2019). The metal phase differs slightly from "normal" PMG, with higher Ge and Ga contents but a similar Ni content, which classifies it as an anomalous PMG (Scott, 1977a). This pallasite also contains large olivine-free regions.
Pavlodar (PMG-am): has rounded olivines, with linear features in three directions ([001], [010], and [100]) at the centre (absent in the outer parts), which may be exsolution features due to the high Cr content (Steele, 1994). It was described as "unique" by Scott (1977a) and classified as PMG-am because its metal has lower Au and As and higher Ir and Ge concentrations than the other PMG. Owing to these compositional differences, some authors suggested that it may either be derived from a different asteroid than PMG (Scott and Taylor, 1990) or formed in a different environment (Wasson and Choi, 2003).

PES:

Eagle Station (PES): has fragmental and angular olivines with rounded microstructures (some very small olivine fragments have been rounded), with significant size variations (Scott, 1977). Together with Cold Bay, Itzawisis, Karavannoe, and Oued Bourdim 001, it forms the PES group, whose O isotopic composition is very distinct from PMG (Fig. S-1).
Karavannoe (PES; MB 101): has less olivine than other PES (60 vol% in Karavannoe; 75–80 vol% in other PES), with olivine occurring as large fractured, angular grains (0.5–2 cm in diameter) and small rounded grains (up to 1 mm) (Teplyakova *et al.*, 2022). Fractures are filled with weathering products, particularly Fe,Ni hydroxide. Karavannoe also contains pyroxene in the form of small or large grains (30 µm to 2 mm), rims along the olivine margins, and inclusions. It is usually assumed that PMG and PES exclusively contain pyroxene as sympletic intergrowths (Buseck, 1977); however, Karavannoe deviates from this pattern.

Ungrouped pallasites:

Vermillion (ungrouped - pyroxene pallasite; MB 80): contains 86 vol% of metal, 14 vol% of silicates, which consist of 93 % olivine, 4.9 % low-Ca orthopyroxene, and 0.1 % augite, 1.5 % chromite, and 0.5 % merrillite (Boesenberg *et al.*, 2000). The presence of low-Ca and high-Ca pyroxenes as large single grains, inclusions in olivine and other pyroxenes, and grains along the margins of olivine, classifies it as a pyroxene pallasite. In the sample used for this study, pyroxene only occurs along the margins of the olivines. The olivines in Vermillion are rounded to subrounded, and occur in "undulatory bands". The olivine composition is similar to that of PMG ($Fa_{11.1-12.1}$), but the metal has different concentrations of siderophile trace elements. The O isotopic composition of Vermillion also differs from that of PES and PMG (Fig. S-1), suggesting that it originates from a different parent body.
NWA 10019 (ungrouped - pyroxene pallasite; MB 104): contains ~50 % olivine, ~10 % orthopyroxene, ~20 % taenite, ~15 % kamacite, with minor calcic plagioclase, troilite, chromite, and calcium-magnesium phosphates (Agee and Ziegler, 2015). The presence of pyroxene and plagioclase makes it a unique pallasite. Its olivines are subhedral to angular, and richer in Fe than those of PMG ($Fa_{16.8\pm0.2}$). The O isotopic composition differs from that of Vermillion (Fig. S-1), suggesting that they originate from different parent bodies (Gregory *et al.*, 2016). Pyroxene occurs as orthopyroxene

grains up to 5 mm, and as small clinopyroxene inclusions within orthopyroxene. NWA 10019 is one of only two known pallasites containing plagioclase, which occurs as single coarse grains in orthopyroxene and olivine, and as fine-grained inclusions within orthopyroxene (Boesenberg *et al.*, 2016). Its metal composition is anomalous, lying outside the ranges defined for the pallasite field and the IIIAB iron trend, owing to its very low Ge (7.7 µg/g) and Ga (9.1 µg/g) concentrations at 9.3 wt% Ni (Boesenberg *et al.*, 2016).

Milton (ungrouped; MB 87): has small olivines (< 5 mm in diameter), mostly in the range of 0.5 to 2 mm, which are subrounded in section but angular to irregular in hand samples (McCoy *et al.*, 2019). These olivines have a unique O isotopic composition among pallasites (Fig. S-1), suggesting that Milton originates from a different parent body than PMG and PES (Jones *et al.*, 2003). The metal phase exhibits kamacite spindles, is Ni-rich (19.2 ± 4.4 wt%), and indicates a faster cooling rate than that of most other pallasites (McCoy *et al.*, 2019).

IIIAB iron meteorites are medium octahedrites composed of taenite and kamacite, along with minor schreibersite and sulfide inclusions (Krot *et al.*, 2014). Their bulk Ni concentrations range from 7 to 10.5 % (Krot *et al.*, 2014). They form the largest group of iron meteorites and originate from the core of a single differentiated parent body, as indicated by their chemical compositions, which display fractional crystallisation trends (Wasson and Choi, 2003). The five IIIAB iron meteorites analysed in this study were selected to represent varying degrees of evolution within these fractional crystallisation trends, from least to most evolved: **Trenton** and **Cape York**, **Owens Valley**, **Grant**, and **Bear Creek**.

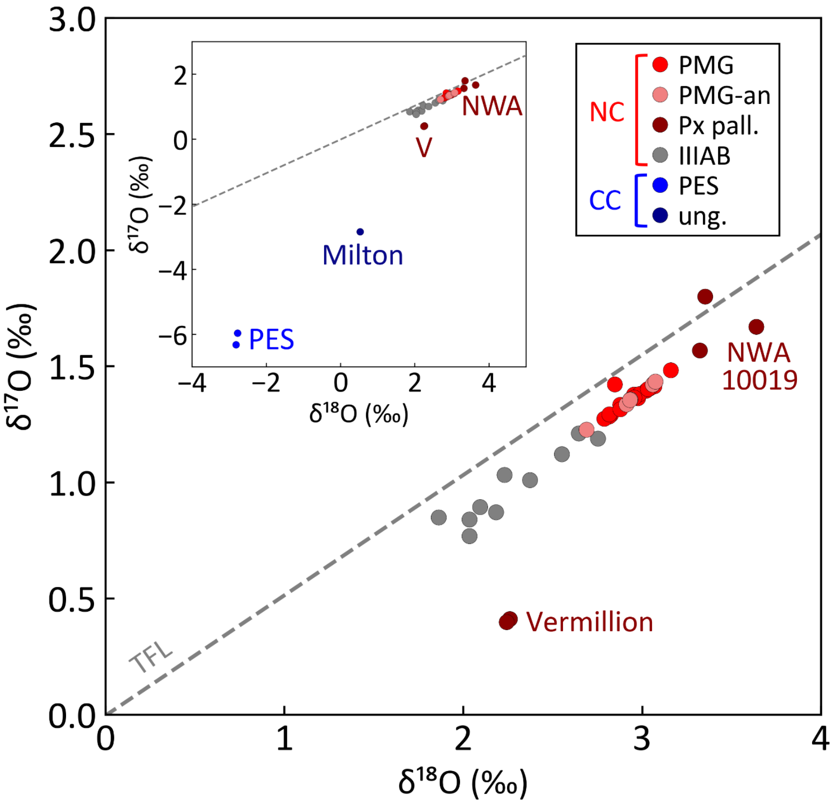

Figure S-1 Oxygen isotopic composition of non-carbonaceous (NC) and carbonaceous (CC) pallasite silicates and oxygen-bearing phases (including chromite, silicates, and phosphates) in IIIAB iron meteorites. Adapted from Boesenberg *et al.* (2012). TFL: Terrestrial fractionation line; Px pall.: pyroxene pallasites; ung.: ungrouped pallasites. Data from: Clayton and Mayeda, 1978; Clayton, 1993; Jones *et al.*, 2003; Bunch *et al.*, 2005; Agee and Ziegler, 2015 (NWA 10019); Greenwood *et al.*, 2015 (PMG).

Detailed Methodology

Sample preparation

Pallasite and iron meteorite samples were obtained as slices or small fragments. Great care was taken to prepare high-purity olivine separates and metal fragments for nitrogen (N) and noble gas analysis. To this end, bulk slices or fragments of pallasites were first cut using a diamond wire saw with ethanol to isolate pieces of the required mass. Metal and silicate phases of each piece were separated by gently tapping along the metal-silicate interfaces with a mallet, exploiting their inherent fragility. Metal and mixed olivine-metal grains were further separated with a hand magnet. Pure fragments were then selected under a binocular microscope, and suitable metal portions were cut with a wire cutter. Special care was taken to select visually pure phases, ensuring no visible signs of other phases, alteration, or inclusions. Where possible, between 4 and 5 mg of olivine and between 5 and 10 mg of metal were selected for analysis. The precise mass of each analysed sample is provided at https://doi.org/10.24396/ORDAR-187 (Gamblin *et al.*, 2025).
Notably, most samples required a cleaning protocol to remove surface oxidation before analysis. Some metal fragments were placed into an ultrasonic bath with 0.2 M HNO_3 for 3 minutes to dissolve the oxidised layer, then rinsed briefly with ultrapure water and subsequently immersed in acetone for 5 minutes. This process was repeated several times for highly oxidised samples, such as Brenham (Fig. S-2). Certain olivine fragments also exhibited surface oxidation. These were cleaned using 6 M HCl at 70 °C for 2–3 minutes (following the protocol of Ali *et al.*, 2018), and rinsed three times with ultrapure water in an ultrasonic bath. A summary of the preparation protocol applied to each sample is provided in Table S-1. All samples underwent at least ultrasonic cleaning with acetone and were dried in a laminar flow hood before being placed into the laser chamber for analysis.

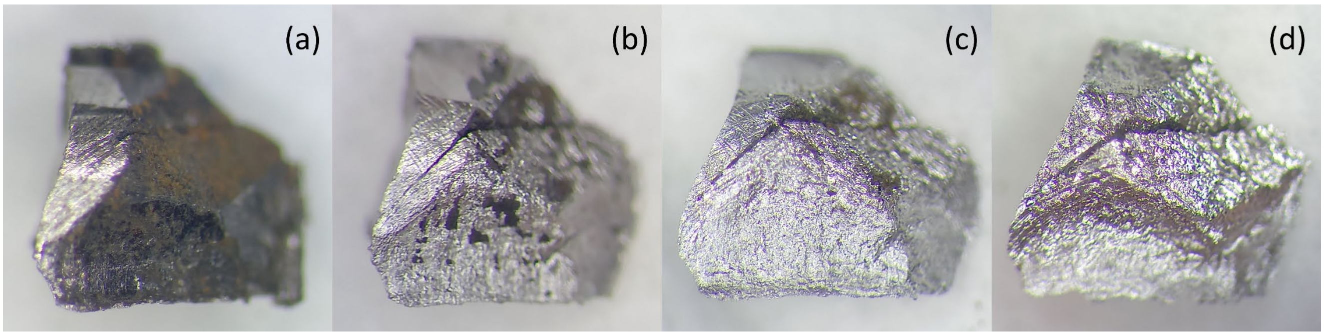

Figure S-2 Effect of the HNO_3 (0.2 M) cleaning protocol on the surface oxidation of a Brenham pallasite metal fragment: (a) sample before treatment, and (b-d) after one, two, and four nitric acid treatments, respectively. The sample is about 2 mm wide.

Table S-1 Pallasites and iron meteorites analysed in this study, and their preparation protocol. Pallasites were either purchased from reputable meteorite dealers or provided by museum collections, including: USNM: United States National Museum (Smithsonian Institution); ASU: Arizona State University; BM: British Museum.

Meteorite	Classification	Source	Number of analyses		HCl treatment for olivine	HNO_3 treatment for metal
			olivine	metal		
Admire	PMG	Meteorite dealer (unknown)	1	1	×	×
Brahin	PMG	Royal Museum of Natural History in Brussels; F. Kuntz (WWMeteorites)	1	1		×
Esquel	PMG	F. Kuntz (WWMeteorites)	1	3		×
Fukang	PMG	K. Moritz (Mo's meteorites)	1	2		×
Imilac	PMG	USNM 612 (metal) BM 90240 (olivines)	1	1		×
Seymchan	PMG	D. Kachalin	1	1		×
Brenham	PMG – am	Royal Museum of Natural History in Brussels (metal); D. Stimpson (olivine and metal)	1	3	×	×
Pavlodar	PMG – am	USNM 2988 (metal) and 2615 (olivine)	1	2	×	×
Vermillion	Px pall.	ASU 1484–2	1	1	×	×
NWA 10019	Px pall.	S. Arnold (Meteorite Men)		1		×
Eagle Station	PES	USNM 2752	2	2		×
Karavannoe	PES	ASU 2078–1	1	1	×	×
Milton	ung.	ASU 1672–1	1	1	×	×
Bear Creek	IIIAB	USNM 968a		1		×
Cape York (Agpalilik)	IIIAB	Copenhagen Geological Museum		1		×
Grant	IIIAB	USNM 836		1		
Owens Valley	IIIAB	USNM 623		1		
Trenton	IIIAB	USNM 2173		1		×

Scanning Electron Microscope (SEM) imaging

Elemental distribution maps were acquired for the pyroxene-rich samples (NWA 10019, Vermillion, and Karavannoe), which were received as slices, to precisely characterise their mineralogy and determine whether it was feasible to separate 4 to 5 mg of pyroxene for analysis. Sub-sections were polished to 1 µm using diamond paste with ethanol. Elemental mapping was carried out at the Scanning electron microscope and microprobe facility of the Centre de Recherches Pétrographiques et Géochimiques (CRPG) on a JEOL JSM-6510 SEM equipped with an energy dispersive X-ray (EDX) detector, using a 3 nA primary electron beam accelerated to 15 kV or 20 kV. No coating was applied to avoid contamination. In Vermillion and NWA 10019, pyroxene is present along the edges of the olivines but in insufficient quantity for N and noble gas analyses (Fig. S-3). In Karavannoe, significant charging occurred on the large silicates (up to 9 mm in diameter) due to their low conductivity and the absence of a coating, preventing clear identification of pyroxenes.

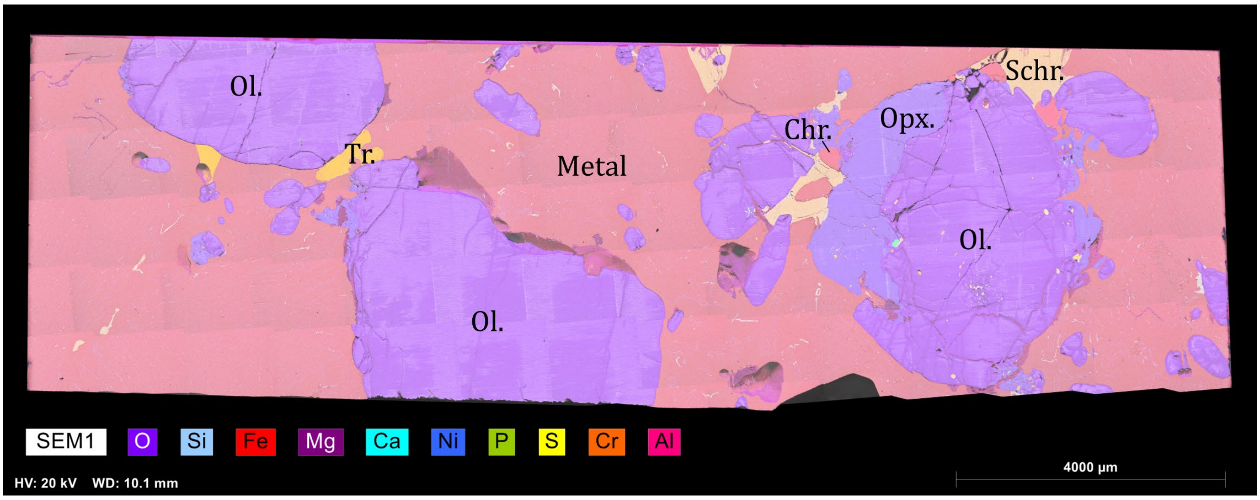

Figure S-3 False-colour, X-ray elemental map of Vermillion (pyroxene pallasite). Orthopyroxene is present along the edges of olivine. Ol: olivine; Tr: troilite; Chr: chromite; Opx: orthopyroxene; Schr: schreibersite.

Noble gas (Ne, Ar) and N analysis

Olivine separates and metal fragments were placed into a ZnSe-windowed laser chamber, which was then connected to the purification line of a Noblesse-HR (3F4M) noble gas mass spectrometer (Nu Instruments) and pumped to ultra-high vacuum (~10^{-9} bar). The laser chamber was baked overnight at ~100 °C to remove adsorbed terrestrial gases from its internal surfaces and the sample surfaces.

Extraction. Noble gases (Ne, Ar) and N were extracted under static vacuum using a CO_2 laser (MIR10^2, Elemental Scientific). A high-resolution CCD video camera positioned above the laser chamber enabled real-time observation of sample heating and melting. In most cases, two extraction steps were performed for the metal phase and three for olivine by progressively increasing the laser power. The first extraction was conducted at low temperature until the sample was slightly heated (as indicated by a faint orange glow) to remove any possible residual surface contamination, despite the laser chamber having been baked overnight. This was generally achieved by increasing the laser power to 15-25 % of the maximum power (32 W). For small olivine fragments, a lower laser power was used for the first step. The second extraction was performed at maximum laser power to extract noble gases and N from the samples. For olivine, a third extraction at maximum laser power ensured complete gas release. A limitation of this method is that the laser was unable to melt the metal phase, potentially preventing complete release of trapped gases. As a result, concentrations (*i.e.* total amounts of Ne, Ar, and N per sample mass) could not be determined for the metal phases, and the discussion mainly focuses on (Ne-Ar-)N isotope ratios.

Purification. After extraction, the gas was divided into two calibrated volumes for separate noble gas (Ne, Ar) and N purification (see the detailed procedures in Zimmermann *et al.*, 2025 and Gamblin *et al.*, 2024). The noble gases were purified in an all-metal line. Argon was first isolated in a charcoal finger held at –196 °C for 5 minutes using liquid nitrogen. Neon and Ar were then sequentially purified using a Ti-sponge getter held at 600 °C for 10 min, followed by two SAES Ti-Al getters at room temperature for 10 min. For Ne purification, a second charcoal finger at liquid nitrogen temperature was used for 10 min to trap residual Ar desorbed from the inner surfaces of the purification line. During the successive Ne and Ar analyses, and for 10 minutes prior to Ne analysis, two GP-50 SAES getters at room temperature connected to the source and detector blocks were used to reduce interfering species, with an additional charcoal finger at liquid nitrogen temperature for Ne only. Nitrogen was purified in a Pyrex and quartz-glass line. Nitrogen, along with other species such as H, C, and S, was oxidised by the O_2 released from heated CuO sticks (450 °C to 900 °C) for 25 min. The oxidised species, except for NO_x, were trapped in a U-shaped cold trap at –180 °C. NO_x was then reduced to molecular nitrogen (N_2) by re-absorbing excess O_2, achieved by gradually cooling the CuO sticks to 300 °C over a 75-minute procedure. A second cold trap, consisting of a glass finger with platinum foils held at –175 °C, was used once the CuO sticks reached 600 °C to further enhance the trapping efficiency of oxidised impurities.

Analysis. Ne, Ar, and N isotopes were analysed successively on the Noblesse-HR noble gas mass spectrometer in multi-collection mode. A trap current of 150 µA and optimized source and zoom optics settings were chosen for each species to maximize sensitivity, minimize instrumental mass fractionation, and ensure high mass resolution and resolving power. Neon isotopes were analysed simultaneously on three ion counters ($^{22}Ne^+$ on IC0, $^{21}Ne^+$ on IC2, $^{20}Ne^+$ on IC3) for 25 cycles. Contributions from interfering species (*e.g.,* $^{40}Ar^{2+}$, $^{20}NeH^+$, and $^{44}CO_2^{2+}$ to $^{20}Ne^+$, $^{21}Ne^+$, and $^{22}Ne^+$, respectively) were minimized by the use of different traps connected to the source and detector blocks. The $^{40}Ar^{2+}$ peak was partially resolved from $^{20}Ne^+$. Only the contribution from $^{44}CO_2^{2+}$ to the $^{22}Ne^+$ signal was corrected. This contribution was estimated by monitoring the $^{44}CO_2^+$ signal during the analysis and using a $^{44}CO_2^{2+}/^{44}CO_2^+$ ionization ratio of 1.28 %. The correction was found to be negligible (<10 cps). Argon isotopes were analysed on two ion counters and a Faraday detector ($^{40}Ar^+$ on Fa0 [10^{11} Ω], $^{38}Ar^+$ on IC2, $^{36}Ar^+$ on IC3) for 25 cycles. The getters used during the analyses maintained a low H_2 level and minimised the $H^{35,37}Cl^+$ signals. The isotopologues of N_2 were analysed on two Faraday detectors and an ion counter ($^{14}N^{14}N^+$ on Fa2 [10^{11} Ω], $^{14}N^{15}N^+$ on Fa1 [10^{12} Ω], and $^{15}N^{15}N^+$ on IC0) for 25 cycles. The $^{12}C^{16}O^+$ signal was measured with the Fa2 Faraday detector to correct for its contribution to the $^{14}N^{14}N^+$ signal. Contributions of $^{13}C^{16}O^+$ and $^{12}C^{18}O^+$ to the $^{14}N^{15}N^+$ and $^{15}N^{15}N^+$ signals, respectively, were then estimated based on the natural abundances of $^{12,13}C$ and $^{16,18}O$. Sensitivity and instrumental mass fractionation were estimated by analysing purified air aliquots at least twice a week during the measurement periods, while procedural blanks were measured prior to the sample analyses. The reproducibility of air standards measurements and the procedural blank values for the different measurement periods are provided in Table S-2.

Table S–2 Reproducibility of air standard measurements and averages of procedural blanks for the different measurement periods.

Measurement period	Reproducibility (%)							Procedural blanks (mol)		
	$^{28}N_2$	$^{28}N_2/^{29}N_2$	^{20}Ne	$^{20}Ne/^{22}Ne$	$^{21}Ne/^{22}Ne$	^{36}Ar	$^{38}Ar/^{36}Ar$	$^{28}N_2$	^{20}Ne	^{36}Ar
01/22 to 05/22	1.96	0.06	0.56	0.37	1.53	1.96	0.21	4.0×10^{-12}	1.7×10^{-16}	1.1×10^{-17}
08/23 to 09/23	5.09	0.08	0.58	0.43	1.47	0.76	0.20	5.7×10^{-12}	2.4×10^{-16}	3.0×10^{-17}
10/23 to 11/23	5.53	0.07	0.41	0.19	1.62	0.13	0.09	3.8×10^{-12}	2.6×10^{-16}	1.3×10^{-17}
07/24 to 08/24	5.19	0.10	0.69	0.25	1.64	0.81	0.44	4.9×10^{-12}	2.3×10^{-16}	3.2×10^{-17}

Data processing. The measured ion signals were corrected for detector baselines and contributions from interfering species, and extrapolated to $t = 0$. Noble gas and N abundances and isotope ratios were calculated by accounting for the sensitivity and the instrumental fractionation of the mass spectrometer and correcting for blank contributions. Nitrogen isotope ratios are reported in the delta notation, where $\delta^{15}N$ (‰) = $\{[1 + 2 \times (^{28}N_2/^{29}N_2)_{atm}] / [1 + 2 \times (^{28}N_2/^{29}N_2)_{measured}] - 1\} \times 1000$, and $(^{28}N_2/^{29}N_2)_{atm}$ is the isotopic composition of atmospheric N_2 (136.05; Nier, 1950). For each metal fragment and olivine separate, total Ne-Ar-N abundances and isotopic ratios were calculated by summing the results from multiple extraction steps. Steps with ≥30 % blank contributions were excluded from these calculations. Nitrogen extracted during the first, low-temperature step from seven metal fragments (three Brenham fragments, the two Pavlodar fragments, the Milton fragment, and a fragment of Esquel; Fig. S-4) exhibited an isotopic composition close to atmospheric ($\delta^{15}N = 0$ ‰), likely reflecting the release of adsorbed atmospheric N_2. This conclusion is supported by the strong oxidation observed for the Brenham and Pavlodar samples prior to acid treatment (see Fig. S-2 for Brenham). Consequently, values from the first step were excluded from the total calculations for these seven samples. All data are available for download at https://doi.org/10.24396/ORDAR-187 (Gamblin *et al.*, 2025).

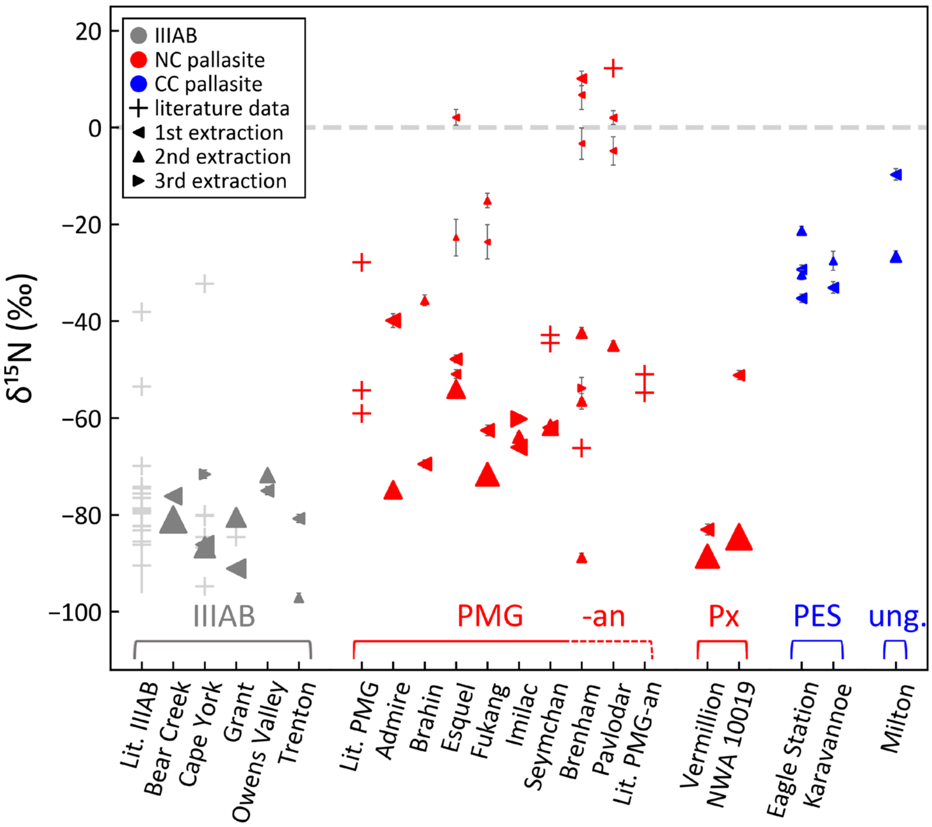

Figure S-4 Nitrogen isotopic composition ($\delta^{15}N$) measured for each extraction step performed on the metal phases of pallasites and IIIAB iron meteorites. Symbol sizes are correlated to the N abundances extracted. Uncertainties are 1σ. Literature data (crosses): Pepin and Becker, 1982; Prombo and Clayton, 1993; Franchi *et al.*, 1993; Murty and Marti, 1994; Sugiura, 1998; Mathew *et al.*, 2000; Murty *et al.*, 2019.

Correction for the cosmogenic ^{15}N contribution

Neon extracted from pallasite metal fragments and olivine separates in this study, as well as in earlier work (*e.g.*, Schultz and Franke, 2004), is predominantly cosmogenic, as evidenced by $^{20}Ne/^{22}Ne$ and $^{21}Ne/^{22}Ne$ ratios near unity (Fig. S-5). While the cosmogenic ^{15}N contribution to the measured $\delta^{15}N$ in metals is expected to be negligible because of the absence of O, this can be verified by calculating the amount of $^{15}N_{cosm}$ produced in pallasite metal, assuming that the total amount of ^{21}Ne extracted is cosmogenic and using a $(^{15}N/^{21}Ne)_{cosm}$ ratio of 1.25 (Mathew *et al.*, 2000). In this case, the magnitude of the $\delta^{15}N$ correction is smaller than the analytical uncertainty of the $\delta^{15}N$ value for each sample. It should be noted, however, that not all the ^{21}Ne may have been extracted from the metal which could result in slight underestimation of these corrections. Using the cosmic ray exposure (CRE) ages derived from olivines (Table S–3) and the equations provided by Herzog *et al.* (2014)—slightly beyond their specified limits (*i.e.* $P_{21\ olivine} = 9.59 - 13.51 \times (^{22}Ne/^{21}Ne) + 4.51 \times (^{22}Ne/^{21}Ne)^2$ for $^{22}Ne/^{21}Ne > 1.06$ and meteoroid radius $R < 100$ cm; $P_{21\ olivine}/P_{21\ metal} = 90$)—and Mathew *et al.* (2000) ($P_{15\ metal} = 1.25 \times P_{21\ metal}$), the calculated $^{15}N_{cosm}$ corrections for metal are also smaller than the uncertainty of the $\delta^{15}N$ values, except for one fragment of Fukang, whose $\delta^{15}N$ value is considered an outlier due to the small amount of N released (see main text). Recoil implantation provides a potential additional source of spallogenic ^{15}N in metal, as ^{15}N produced in silicates can be implanted into the metal surface when metal and silicate grains are intimately intergrown (Mathew *et al.*, 2005). However, in the pallasite metal samples of this study, which contain large silicate-free metal areas and whose surfaces were cleaned in a dilute HNO_3 (0.2 N) bath that removed their surface layer, any such recoil implantation is negligible.

In contrast, the proportion of $^{15}N_{cosm}$ in olivine is significant due to the large production cross-sections for N isotopes from O (Mathew and Murty, 1993) and the low abundance of trapped N in olivine. Olivine separates with the highest $^{21}Ne_{cosm}$ concentrations (and the highest CRE ages) also exhibit the highest $\delta^{15}N$ values (Fig. S-6). Correcting for cosmogenic ^{15}N contributions in pallasite olivine based on Ne-Ar analyses is challenging because cosmogenic nuclide production rates depend on several factors, including the chemical composition of the sample, the size of the meteoroid in space, and the shielding depth. Additionally, different isotopic systems may yield varying CRE ages for the same sample (Schultz and Franke, 2004; Herzog *et al.*, 2014). The calculated CRE ages, reported in Table S–3 (derived using the equation for $P_{21\ olivine}$ from Herzog *et al.*, 2014), show a significant range of values, mirroring the variability in the literature. This variability raises questions about the reliability and precision of CRE age determinations and underscores the inherent challenges in applying these corrections for cosmic ray exposure. However, $\delta^{15}N$ can be corrected for cosmogenic ^{15}N without calculating CRE ages, by applying a $(^{15}N/^{21}Ne)_{cosm}$ production ratio. The resulting ranges of corrected $\delta^{15}N$ values for olivine are provided in Table S–4, calculated using the range of $(^{15}N/^{21}Ne)_{cosm}$ production ratios reported by Mathew and Murty (1993) for olivine in meteoroids exposed to galactic cosmic rays (*i.e.* $(^{15}N/^{21}Ne)_{cosm}$ = 2.9 to 5.2). In most cases, these corrections are substantial—up to several hundred per mil—and prevent a clear determination of whether the $\delta^{15}N$ values of olivine and metal in pallasites differ. For the N-rich olivines of PES (Eagle Station and Karavannoe), the magnitude of the correction is smaller, resulting in a more constrained range of corrected $\delta^{15}N$ values. While olivine appears to be enriched in ^{15}N compared to the metal phase in PES, the inherent uncertainties of the corrections make it difficult to draw definitive conclusions about a possible N isotopic difference.

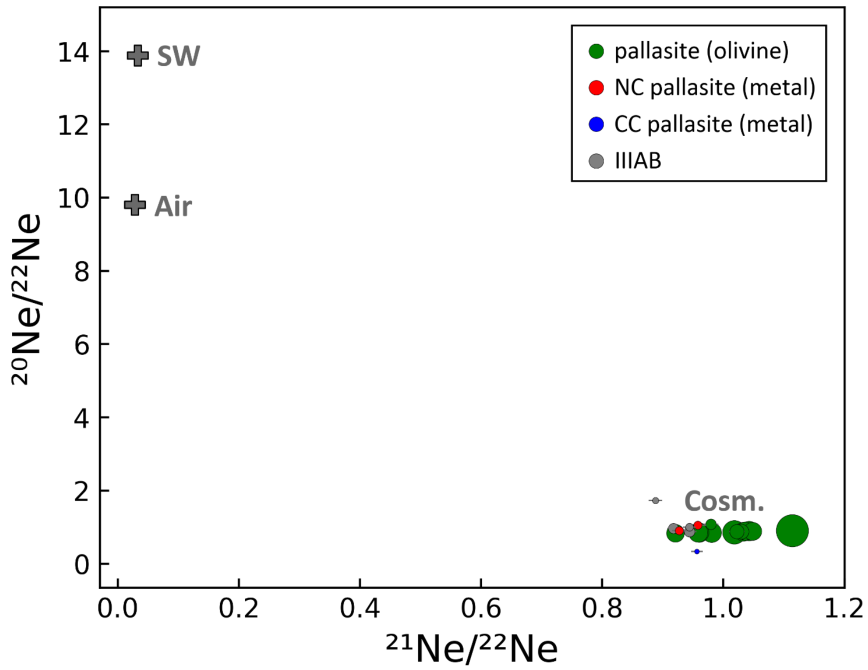

Figure S-5 Isotopic composition of Ne extracted from pallasites and iron meteorites. Symbol sizes are correlated to the extracted ^{21}Ne abundances. The isotopic signatures of the solar wind (SW; $^{20}Ne/^{22}Ne$ = 13.87 and $^{21}Ne/^{22}Ne$ = 0.033; Ott, 2014 (mean)), the terrestrial atmosphere (Air; $^{20}Ne/^{22}Ne$ = 9.80 and $^{21}Ne/^{22}Ne$ = 0.0285; Honda *et al.*, 2015), and the cosmogenic endmember (Cosm.; $^{20}Ne/^{22}Ne \approx 1$ and $^{21}Ne/^{22}Ne \approx 1$; Wieler, 2002) are shown for comparison.

Table S-3 ^{21}Ne concentrations in olivine and cosmic ray exposure (CRE) ages of pallasites.

	^{21}Ne[a] [10^{-12} mol/g]	^{21}Ne[b] [10^{-12} mol/g]	CRE ages[a] [Myr]	CRE ages[c] [Myr]	CRE ages range[d] [Myr]
Admire	22.23 ± 0.33	15.62 ± 0.67	74.17	38 ± 6 39 ± 6	38 ± 6 to 113 ± 12
Brahin	9.59 ± 0.12	30.34 30.25	29.05	108 ± 16	108 ± 16
Esquel	3.42 ± 0.04	3.83 3.15	10.66	12 ± 2	11 ± 1 to 14 ± 1
Fukang	10.90 ± 0.15		31.28		
Imilac	7.55 ± 0.10	30.65	22.51	72 ±11 110 ± 17	42 ± 3 to 110 ± 17
Seymchan	0.68 ± 0.01		3.07	30 ± 4	30 ± 4
Brenham	5.78 ± 0.08	16.28 ± 0.89 to 1.08	18.73		156 ± 8
Pavlodar	9.63 ± 0.12		42.76		
Vermillion	85.12 ± 1.31		174.12		
Eagle Station	10.15 ± 0.14 11.91 ± 0.19	8.79 ± 0.45	56.13 64.84	35	35 to 71 ± 5
Karavannoe	7.67 ± 0.13		15.19		
Milton	18.28 ± 0.31		172.22		

a) This study; b) Eberhardt and Eberhardt (1961), Megrue (1968), Schultz and Franke (2004), and references therein; c) CRE ages calculated based on Ne isotopes (Herzog *et al.*, 2014); d) range of CRE ages calculated with different isotopic systems (Herzog *et al.*, 2014).

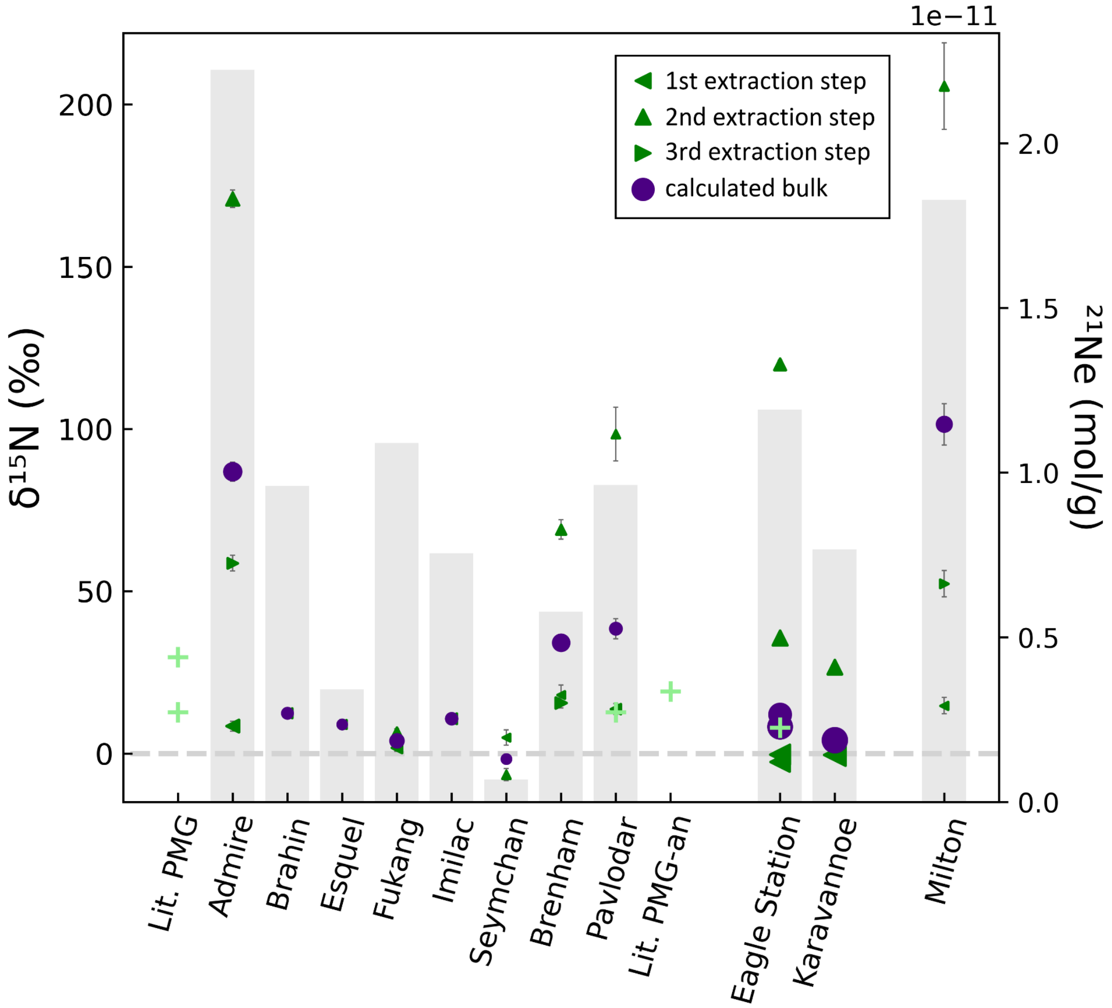

Figure S-6 $\delta^{15}N$ values without correction for the cosmogenic ^{15}N contribution (filled symbols) and ^{21}Ne concentrations (gray bars) of pallasite olivine. Green triangles represent the $\delta^{15}N$ values measured for each extraction step, whereas purple filled circles show the summed $\delta^{15}N$ values of the samples, calculated as weighted averages of the extraction steps. Symbol sizes are correlated to the N abundances extracted. The dashed line indicates the $\delta^{15}N$ value of atmospheric N_2 ($\delta^{15}N = 0$ ‰). Vermillion and NWA 10019 are not shown here because N extracted from the Vermillion olivine separate had a blank contribution >30 %, and pure olivine grains could not be selected from NWA 10019. Literature data (green crosses) are from Prombo and Clayton (1993).

Table S-4 Non-spallation-corrected $\delta^{15}N$ values of metal and olivine in pallasites, and spallation-corrected $\delta^{15}N$ values of olivine. Corrections for the cosmogenic ^{15}N contributions were applied using the range of $(^{15}N/^{21}Ne)_{cosm}$ production ratios from Mathew and Murty (1993) for olivine in meteoroids exposed to galactic cosmic rays (*i.e.* 2.9 to 5.2). no cor.: no cosmogenic correction; cor. min.: corrected with the lowest production ratio; cor. max.: corrected with the highest production ratio.

	$\delta^{15}N_{metal}$ (‰)	$\delta^{15}N_{olivine}$ (‰) (no cor.)	$\delta^{15}N_{olivine}$ (‰) (cor. min.)	$\delta^{15}N_{olivine}$ (‰) (cor. max.)
Admire	–65.09 ± 1.20	86.83 ± 2.92	–41.16	–142.70
Brahin	–66.63 ± 0.77	12.39 ± 1.19	–371.57	–676.08
Esquel	–48.95 ± 0.89 –53.20 ± 1.09	8.91 ± 1.51	–214.36	–391.43
Fukang	–17.38 ± 1.44 –70.86 ± 1.02	3.92 ± 0.78	–175.13	–317.15
Imilac	–63.20 ± 0.51	10.71 ± 1.07	–231.07	–422.83
Seymchan	–61.96 ± 0.59	-1.74 ± 1.49	–45.55	–80.30
Brenham	–47.94 ± 0.96 –56.57 ± 1.19 –88.86 ± 0.90	34.13 ± 1.67	–6.55	–38.80
Pavlodar	–45.04 ± 0.91	38.42 ± 3.15	–231.81	–446.13
Vermillion	–88.11 ± 1.02			
NWA 10019	–83.67 ± 0.92			
Eagle Station	–26.12 ± 0.64 –34.03 ± 0.69	8.29 ± 0.71 12.00 ± 0.85	–10.12 –10.53	–24.73 –28.40
Karavannoe	–32.11 ± 1.05	4.10 ± 0.89	–6.57	–15.04
Milton	–26.67 ± 0.71	101.44 ± 6.36	–85.16	–233.17

Supplementary figure

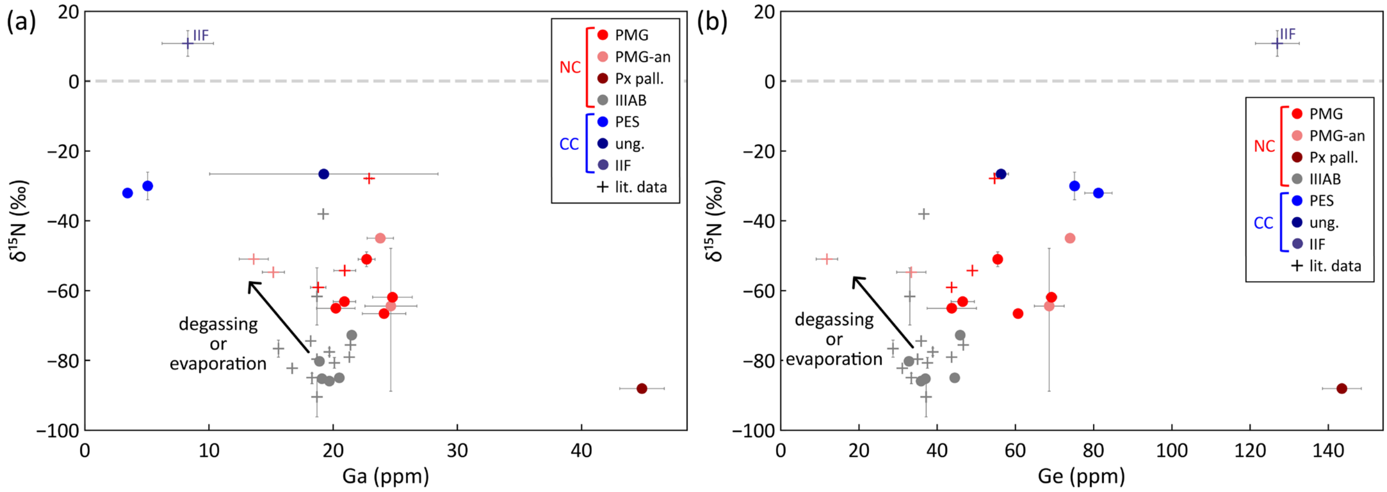

Figure S-7 $\delta^{15}N$ values of pallasite metals and IIIAB iron meteorites as a function of their (a) Ga and (b) Ge concentrations. Ge and Ga are moderately volatile siderophile elements, with Ge being more volatile (50% condensation temperatures: 830 K for Ge and 1010 K for Ga; Wood *et al.*, 2019). The better-defined correlations observed for Ge compared to Ga may reflect this difference in volatility. However, evaporation or degassing of metal alloy is expected to produce negative correlations between $\delta^{15}N$ and Ge-Ga concentrations in metal samples originating from the same parent body core (*e.g.*, IIIAB and PMG), as Ge-Ga loss would be accompanied by preferential loss of isotopically light N; the expected directions of these trends are indicated by arrows. Additional kinetic processes are therefore required to account for the positive $\delta^{15}N$-[Ge, Ga] correlations observed from IIIAB to PMG, if they derive from a common planetesimal core. IIF irons are also shown here because of their chemical similarities with PES, although they likely originate from a different parent body (Kracher *et al.*, 1980). $\delta^{15}N$ values represent averages of data obtained in this study or compiled from the literature. Error bars on $\delta^{15}N$ correspond to the range of values when multiple data points are available, or to the 1σ analytical uncertainty when only a single value is reported. Ge and Ga concentrations for pallasites and IIF irons are literature averages, with error bars corresponding to one standard deviation. For IIIAB iron meteorites, Ge and Ga concentration are taken from Chabot and Zhang (2022), for which no associated uncertainties were reported. Literature data sources are listed in Table S-5.

Supplementary table

Table S-5 Literature sources for $\delta^{15}N$ values, O isotopic anomalies, Mo nucleosynthetic anomalies, and Ge and Ga concentrations cited for pallasites and iron meteorites.

	Data source		Data compilation
	Pallasite	Iron meteorite	
$\delta^{15}N$	Prombo and Clayton, 1993 Mathew *et al.*, 2000	Pepin and Becker, 1982 Prombo and Clayton, 1993 Franchi *et al.*, 1993 Murty and Marti, 1994 Sugiura, 1998 Mathew *et al.*, 2000 Sugiura *et al.*, 2000 Ponganis and Marti, 2007 Murty *et al.*, 2019	https://doi.org/10.24396/ORDAR-185, Füri and Gamblin (2025)
O	Clayton and Mayeda, 1996 Jones *et al.*, 2003 Bunch *et al.*, 2005 Greenwood *et al.*, 2006 Agee and Ziegler, 2015 Greenwood *et al.*, 2015 Ali *et al.*, 2018 Teplyakova *et al.*, 2022 Windmill *et al.*, 2022	Clayton and Mayeda, 1996 Wang *et al.*, 2004 Franchi, 2008 Franchi *et al.*, 2013 Van Roosbroek *et al.*, 2015 McDermott *et al.*, 2016	Greenwood *et al.*, 2017
$\Delta^{95}Mo$	Burkhardt *et al.*, 2011 Hilton *et al.*, 2019 Kruijer *et al.*, 2022	Kruijer *et al.*, 2017 Poole *et al.*, 2017 Bermingham *et al.*, 2018 Worsham *et al.*, 2019 Yokoyama *et al.*, 2019 Spitzer *et al.*, 2020	Spitzer *et al.*, 2020
Ge	Lovering *et al.*, 1957 Smales *et al.*, 1967 Wasson and Kimberlin, 1967 Wasson and Sedwick, 1969 Scott and Wasson, 1976 Scott, 1977 Wasson and Wang, 1986 Ulff-Moller *et al.*, 1997 Boesenberg *et al.*, 2000 Wasson and Kallemeyn, 2002 Wasson and Choi, 2003 Hillebrand, 2004 McCoy *et al.*, 2019 Teplyakova *et al.*, 2022	Wasson, 1969 Scott and Wasson, 1973 Easton and Elliott, 1977 Esbensen *et al.*, 1982 Wasson *et al.*, 1998 Wasson and de Bon, 1998 Wasson, 1999	Chabot and Zhang, 2022

Table S-5 Continued.

	Data sources		Data compilations
	Pallasites	Iron meteorites	
Ga	Lovering *et al.*, 1957 Smales *et al.*, 1967 Wasson and Kimberlin, 1967 Wasson and Sedwick, 1969 Scott and Wasson, 1976 Scott, 1977 Wasson and Wang, 1986 Krot *et al.*, 1992 Boesenberg *et al.*, 1995 Choi and Wasson, 1996 Ulff-Moller *et al.*, 1997, 1998 Boesenberg *et al.*, 2000 Wasson and Kallemeyn, 2002 Jones *et al.*, 2003 Russell *et al.*, 2003 Wasson and Choi, 2003 Hillebrand, 2004 McCoy *et al.*, 2019 Teplyakova *et al.*, 2022	Cobb, 1966 Wasson, 1969 Scott and Wasson, 1973 Easton and Elliott, 1977 Esbensen *et al.*, 1982 Wasson *et al.*, 1998 Wasson and De Bon, 1998 Wasson, 1999	Chabot and Zhang, 2022

Supplementary Information References

Agee, C.B., Ziegler, K., Muttik, N. (2015) New Unique Pyroxene Pallasite: Northwest Africa 10019. *78th Annual Meeting of the Meteoritical Society*, 5084. https://www.hou.usra.edu/meetings/metsoc2015/pdf/5084.pdf

Ali, A., Jabeen, I., Banerjee, N.R., Osinski, G.R., Nicklin, I., Gregory, D., Herrmann, P. (2018) The oxygen isotope compositions of olivine in main group (MG) pallasites: New measurements by adopting an improved laser fluorination approach. *Meteoritics & Planetary Science* 53, 1223–1237. https://doi.org/10.1111/maps.13072

Bermingham, K.R., Worsham, E.A., Walker, R.J. (2018) New insights into Mo and Ru isotope variation in the nebula and terrestrial planet accretionary genetics. *Earth and Planetary Science Letters* 487, 221–229. https://doi.org/10.1016/j.epsl.2018.01.017

Boesenberg, J.S., Prinz, M., Weisberg, M.K., Davis, A.M., Clayton, R.N., Mayeda, T.K., Wasson, J.T. (1995) Pyroxene Pallasites: A New Pallasite Grouplet. *Meteoritics* 30, 488–489

Boesenberg, J.S., Davis, A.M., Prinz, M., Weisberg, M.K., Clayton, R.N., Mayeda, T.K. (2000) The pyroxene pallasites, Vermillion and Yamato 8451: Not quite a couple. *Meteoritics & Planetary Science* 35, 757–769. https://doi.org/10.1111/j.1945-5100.2000.tb01460.x

Boesenberg, J.S., Delaney, J.S., Hewins, R.H. (2012) A petrological and chemical reexamination of Main Group pallasite formation. *Geochimica et Cosmochimica Acta* 89, 134–158. https://doi.org/10.1016/j.gca.2012.04.037

Boesenberg, J.S., Mayne, R.G., Humayun, M., Silver, A.P., Greenwood, R.C., Franchi, I.A. (2016) Pyroxene-Plagioclase Pallasite Northwest Africa 10019: Where Does It Belong? *47th Lunar and Planetary Science Conference,* 2297. https://www.hou.usra.edu/meetings/metsoc2015/pdf/5084.pdf

Buchwald, V.F. (1975) The minerals and structural components of iron meteorites. In: Scott, E. (Ed) *Handbook of iron meteorites*, Volume 1. University of California Press, Berkeley, Los Angeles, California, 87–113

Bunch, T.E., Rumble, D., Wittke, J.H., Irving, A.J. (2005) Pyroxene-rich pallasites Zinder and NWA 1911: not like the others. *Meteoritics & Planetary Science* 40, 5219

Burkhardt, C., Kleine, T., Oberli, F., Pack, A., Bourdon, B., Wieler, R. (2011) Molybdenum isotope anomalies in meteorites: Constraints on solar nebula evolution and origin of the Earth. *Earth and Planetary Science Letters.* https://doi.org/10.1016/j.epsl.2011.10.010

Buseck, P.R. (1977) Pallasite meteorites—mineralogy, petrology and geochemistry. *Geochimica et Cosmochimica Acta* 41, 711–740. https://doi.org/10.1016/0016-7037(77)90044-8

Buseck, P.R., Goldstein, J.I. (1969) Olivine Compositions and Cooling Rates of Pallasitic Meteorites. *Geological Society of America Bulletin* 80, 2141. https://doi.org/10.1130/0016-7606(1969)80[2141:OCACRO]2.0.CO;2

Chabot, N.L., Zhang, B. (2022) A revised trapped melt model for iron meteorites applied to the IIIAB group. *Meteoritics & Planetary Science* 57, 200–227. https://doi.org/10.1111/maps.13740

Choi, B.-G., Wasson, J.T. (1996) Pallasites - chemical compositions and relationship to IIIAB irons. *27th Lunar and Planetary Science Conference,* 1112. https://www.lpi.usra.edu/meetings/lpsc1996/pdf/1112.pdf

Clayton, R.N. (1993) Oxygen Isotopes in Meteorites. *Annual Review of Earth and Planetary Sciences* 21, 115–149.

Clayton, R.N., Mayeda, T.K. (1978) Genetic relations between iron and stony meteorites. *Earth and Planetary Science Letters* 40, 168–174. https://doi.org/10.1016/0012-821X(78)90087-0

Cobb, J.C. (1966) A trace element study of iron meteorites. *Journal of Geophysical Research* 72, 1329–1341. https://doi.org/10.1029/JZ072i004p01329

Easton, A.J., Elliott, C.J. (1977) Analyses of some meteorites from the British Museum (Natural History) collection. *Meteoritics* 12, 409–416. https://doi.org/10.1111/j.1945-5100.1977.tb00459.x

Eberhardt, P., Eberhardt, A. (1961) Ne in some Stone Meteorites. *Zeitschrift für Naturforschung A* 16, 236–238. https://doi.org/10.1515/zna-1961-0304

Esbensen, K.H., Buchwald, V.F., Malvin, D.J., Wasson, J.T. (1982) Systematic compositional variations in the Cape York iron meteorite. *Geochimica et Cosmochimica Acta* 46, 1913–1920. https://doi.org/10.1016/0016-7037(82)90129-6

Franchi, I.A. (2008) Oxygen Isotopes in Asteroidal Materials. *Reviews in Mineralogy and Geochemistry* 68, 345–397. https://doi.org/10.2138/rmg.2008.68.13

Franchi, I.A., Wright, I.P., Pillinger, C.T. (1993) Constraints on the formation conditions of iron meteorites based on concentrations and isotopic compositions of nitrogen. *Geochimica et Cosmochimica Acta* 57, 3105–3121. https://doi.org/10.1016/0016-7037(93)90297-A

Franchi, I.A., Greenwood, R.C., Scott, E.R.D. (2013) The IIIAB-Pallasite relationship revisited: the oxygen isotope perspective. *76th Annual Meteoritical Society Meeting,* 5326. https://www.hou.usra.edu/meetings/metsoc2013/pdf/5326.pdf

Füri, E., Gamblin, J. (2025) Compilation of nitrogen isotope ratios and abundances in iron meteorites determined by step-heating or secondary ion mass spectrometry (SIMS). *OTELo Research Data Repository, ORDaR.* https://doi.org/10.24396/ORDAR-185

Gamblin, J., Füri, E., Marty, B., Zimmermann, L., Bekaert, D.V. (2024) Dissecting the complex Ne-Ar-N signature of asteroid Ryugu by step-heating analysis. *Geochemical Perspectives Letters* 31, 44–48. https://doi.org/10.7185/geochemlet.2431

Gamblin, J., Füri, E., Luais, B., Zimmermann, L. (2025) N-Ne-Ar data for pallasites and IIIAB iron meteorites. *OTELo Research Data Repository, ORDaR.* https://doi.org/10.24396/ORDAR-187

Greenwood, R.C., Franchi, I.A., Jambon, A., Barrat, J.A., Burbine, T.H. (2006) Oxygen Isotope Variation in Stony-Iron Meteorites. *Science* 313, 1763–1765. https://doi.org/10.1126/science.1128865

Greenwood, R.C., Barrat, J.A., Scott, E.R.D., Haack, H., Buchanan, P.C., *et al.* (2015) Geochemistry and oxygen isotope composition of main-group pallasites and olivine-rich clasts in mesosiderites: Implications for the "Great Dunite Shortage" and HED-mesosiderite connection. *Geochimica et Cosmochimica Acta* 169, 115–136. https://doi.org/10.1016/j.gca.2015.07.023

Greenwood, R.C., Burbine, T.H., Miller, M.F., Franchi, Ian.A. (2017) Melting and differentiation of early-formed asteroids: The perspective from high precision oxygen isotope studies. *Geochemistry* 77, 1–43. https://doi.org/10.1016/j.chemer.2016.09.005

Gregory, J.D., Mayne, R.G., Boesenberg, J.S., Humayun, M., Silver, A.P., Franchi, I.A. (2016) Choteau Makes Three: A Characterization of the Third Member of the Vermillion Subgroup. *47th Lunar and Planetary Science Conference,* 2393. https://www.hou.usra.edu/meetings/lpsc2016/pdf/2393.pdf

Herzog, G.F., Cook, D.L., Cosarinsky, M., Huber, L., Leya, I., Park, J. (2014) Cosmic-ray exposure ages of pallasites. *Meteoritics & Planetary Science* 50, 86–111. https://doi.org/10.1111/maps.12404

Hillebrand, J.T., McDonough, W.F., Walker, R.J., Piccoli, P.M. (2004) Characterization of the distribution of siderophile and highly siderophile elements in the Milton and Eagle Station pallasites. *35th Lunar and Planetary Science Conference*, 1278. https://www.lpi.usra.edu/meetings/lpsc2004/pdf/1278.pdf

Hilton, C.D., Bermingham, K.R., Walker, R.J., McCoy, T.J. (2019) Genetics, crystallization sequence, and age of the South Byron Trio iron meteorites: New insights to carbonaceous chondrite (CC) type parent bodies. *Geochimica et Cosmochimica Acta* 251, 217–228. https://doi.org/10.1016/j.gca.2019.02.035

Honda, M., Zhang, X., Phillips, D., Hamilton, D., Deerberg, M., Schwieters, J.B. (2015) Redetermination of the 21Ne relative abundance of the atmosphere, using a high resolution, multi-collector noble gas mass spectrometer (HELIX-MC Plus). *International Journal of Mass Spectrometry* 387, 1–7. https://doi.org/10.1016/j.ijms.2015.05.012

Jones, R.H., Wasson, J.T., Larson, T., Sharp, Z.D. (2003) Milton: A new, unique pallasite. *34th Lunar and Planetary Science Conference*, 1683. https://www.lpi.usra.edu/meetings/lpsc2003/pdf/1683.pdf

Krot, A.N., Zaslavskay, N.I., Petaev, M.I., Kononkova, N.N., Kolesov, G.M., Barsukova, L.D. (1992) The Sychevka IIIAB iron meteorite: A new find from Russia. *Meteoritics* 27, 465–466. https://doi.org/10.1111/j.1945-5100.1992.tb00230.x

Krot, A.N., Keil, K., Scott, E.R.D., Goodrich, C.A., Weisberg, M.K. (2014) Classification of Meteorites and Their Genetic Relationships. *Treatise on Geochemistry*. Elsevier, 1–63. https://doi.org/10.1016/B978-0-08-095975-7.00102-9

Kruijer, T.S., Burkhardt, C., Budde, G., Kleine, T. (2017) Age of Jupiter inferred from the distinct genetics and formation times of meteorites. *Proceedings of the National Academy of Sciences* 114, 6712–6716. https://doi.org/10.1073/pnas.1704461114

Kruijer, T.S., Burkhardt, C., Borg, L.E., Kleine, T. (2022) Tungsten and molybdenum isotopic evidence for an impact origin of pallasites. *Earth and Planetary Science Letters* 584, 117440. https://doi.org/10.1016/j.epsl.2022.117440

Lovering, J.F., Nichiporuk, W., Chodos, A., Brown, H. (1957) The distribution of gallium, germanium, cobalt, chromium, and copper in iron and stony-iron meteorites in relation to nickel content and structure. *Geochimica et Cosmochimica Acta* 11, 263–278. https://doi.org/10.1016/0016-7037(57)90099-6

Mathew, K.J., Murty, S.V.S. (1993) Cosmic ray produced nitrogen in extra terrestrial matter. *Journal of Earth System Science* 102, 415–437. https://doi.org/10.1007/BF02841731

Mathew, K.J., Palma, R.L., Marti, K., Lavielle, B. (2000) Isotopic signatures and origin of nitrogen in IIE and IVA iron meteorites. *Geochimica et Cosmochimica Acta* 64, 545–557. https://doi.org/10.1016/S0016-7037(99)00316-6

Mathew, K.J., Marti, K., Kim, Y. (2005) Nitrogen in chondritic metal. *Geochimica et Cosmochimica Acta* 69, 753–762. https://doi.org/10.1016/j.gca.2004.07.027

McCoy, T.J., Corrigan, C.M., Nagashima, K., Reynolds, V.S., Ash, R.D., McDonough, W.F., Yang, J., Goldstein, J.I., Hilton, C.D. (2019) The Milton pallasite and South Byron Trio irons: Evidence for oxidation and core crystallization. *Geochimica et Cosmochimica Acta* 259, 358–370. https://doi.org/10.1016/j.gca.2019.06.005

McDermott, K.H., Greenwood, R.C., Scott, E.R.D., Franchi, I.A., Anand, M. (2016) Oxygen isotope and petrological study of silicate inclusions in IIE iron meteorites and their relationship with H chondrites. *Geochimica et Cosmochimica Acta* 173, 97–113. https://doi.org/10.1016/j.gca.2015.10.014

McKibbin, S.J., Pittarello, L., Makarona, C., Hamann, C., Hecht, L., Chernonozhkin, S.M., Goderis, S., Claeys, P. (2019) Petrogenesis of main group pallasite meteorites based on relationships among texture, mineralogy, and geochemistry. *Meteoritics & Planetary Science* 54, 2814–2844. https://doi.org/10.1111/maps.13392

Megrue, G.H. (1968) Rare gas chronology of hypersthene achondrites and pallasites. *Journal of Geophysical Research* 73, 2027–2033. https://doi.org/10.1029/JB073i006p02027

Murty, S.V.S., Marti, K. (1994) Nitrogen isotopic signatures in Cape York: Implications for formation of Group III A irons. *Geochimica et Cosmochimica Acta* 58, 1841–1848. https://doi.org/10.1016/0016-7037(94)90540-1

Murty, S.V.S., Ghosh, S., Ray, D. (2019) Noble gases and nitrogen in Raghunathpura (IIAB) and Nyaung (IIIAB) iron meteorites. *Meteoritics & Planetary Science* 54, 90–103. https://doi.org/10.1111/maps.13195

Nier, A.O. (1950) A Redetermination of the Relative Abundances of the Isotopes of Carbon, Nitrogen, Oxygen, Argon, and Potassium. *Physical Review* 77, 789–793. https://doi.org/10.1103/PhysRev.77.789

Ott, U. (2014) Planetary and pre-solar noble gases in meteorites. *Geochemistry* 74, 519–544. https://doi.org/10.1016/j.chemer.2014.01.003

Pepin, R.O., Becker, R.H. (1982) Nitrogen Isotopes in Iron Meteorites. *Meteoritics* 17, 269.

Ponganis, K.V., Marti, K. (2007) Nitrogen components in IAB/IIICD iron meteorites. *Meteoritics & Planetary Science* 42, 331–346. https://doi.org/10.1111/j.1945-5100.2007.tb00237.x

Poole, G.M., Rehkämper, M., Coles, B.J., Goldberg, T., Smith, C.L. (2017) Nucleosynthetic molybdenum isotope anomalies in iron meteorites – new evidence for thermal processing of solar nebula material. *Earth and Planetary Science Letters* 473, 215–226. https://doi.org/10.1016/j.epsl.2017.05.001

Prombo, C.A., Clayton, R.N. (1993) Nitrogen isotopic compositions of iron meteorites. *Geochimica et Cosmochimica Acta* 57, 3749–3761. https://doi.org/10.1016/0016-7037(93)90153-N

Russell, S.S., Zipfel, J., Folco, L., Jones, R., Grady, M.M., McCOY, T., Grossman, J.N. (2003) The Meteoritical Bulletin, No. 87, 2003 July. *Meteoritics & Planetary Science* 38. https://doi.org/10.1111/j.1945-5100.2003.tb00328.x

Schultz, L., Franke, L. (2004) Helium, neon, and argon in meteorites: A data collection. *Meteoritics & Planetary Science* 39, 1889–1890. https://doi.org/10.1111/j.1945-5100.2004.tb00083.x

Scott, E.R.D. (1977a) Pallasites—metal composition, classification and relationships with iron meteorites. *Geochimica et Cosmochimica Acta* 41, 349–360. https://doi.org/10.1016/0016-7037(77)90262-9

Scott, E.R.D. (1977b) Formation of olivine-metal textures in pallasite meteorites. *Geochimica et Cosmochimica Acta* 41, 693–710. https://doi.org/10.1016/0016-7037(77)90043-6

Scott, E.R.D., Wasson, J.T. (1973) The chemical classification of iron meteorites—VII. A reinvestigation of irons with Ge concentrations between 25 and 80 ppm. *Geochimica et Cosmochimica Acta* 37, 1957–1983. https://doi.org/10.1016/0016-7037(73)90151-8

Scott, R.D., Wasson, T. (1976) Chemical classification of iron meteorite~VII1. Groups IC. IIE, IIIF and 97 other irons. https://doi.org/10.1016/0016-7037(76)90198-8

Scott, E.R.D., Taylor, G.J. (1990) Origins of pallasites at the core–mantle boundaries of asteroids. *21st Lunar and Planetary Science Conference*, 1568. https://www.lpi.usra.edu/meetings/lpsc1990/pdf/1568.pdf

Smales, A.A., Mapper, D., Fouché, K.F. (1967) The distribution of some trace elements in iron meteorites, as determined by neutron activation. *Geochimica et Cosmochimica Acta* 31, 673–720. https://doi.org/10.1016/S0016-7037(67)80026-7

Spitzer, F., Burkhardt, C., Budde, G., Kruijer, T.S., Morbidelli, A., Kleine, T. (2020) Isotopic Evolution of the Inner Solar System Inferred from Molybdenum Isotopes in Meteorites. *The Astrophysical Journal Letters* 898, L2. https://doi.org/10.3847/2041-8213/ab9e6a

Steele, I. (1994) Chemical Zoning and Exsolution in Olivine of the Pavlodar Pallasite: Comparison with Springwater Olivine. *25th Lunar and Planetary Science Conference*, 1668. https://www.lpi.usra.edu/meetings/lpsc1994/pdf/1668.pdf

Sugiura, N. (1998) Ion probe measurements of carbon and nitrogen in iron meteorites. *Meteoritics & Planetary Science* 33, 393–409. https://doi.org/10.1111/j.1945-5100.1998.tb01645.x

Sugiura, N., Ikeda, Y., Zashu, S., Wasson, T. (2000) Nitrogen-isotopic compositions of IIIE iron meteorites. *Meteoritics & Planetary Science* 35, 749–756. https://doi.org/10.1111/j.1945-5100.2000.tb01459.x

Teplyakova, S.N., Lorenz, C.A., Ivanova, M.A., Humayun, M., Kononkova, N.N., Borisovsky, S.E., Korochantsev, A.V., Franchi, I.A., Zinovieva, N.G. (2022) Karavannoe: Mineralogy, trace element geochemistry, and origin of Eagle Station group pallasites. *Meteoritics & Planetary Science* 57, 1158–1173. https://doi.org/10.1111/maps.13814

Ulff-Moller, F., Tran, J., Choi, B.-G., Haag, R., Rubin, A.E., Wasson, J.T. (1997) Esquel: implications for pallasite formation processes based on the petrography of a large slab. *28th Lunar and Planetary Science Conference*, 1342. https://www.lpi.usra.edu/meetings/lpsc97/pdf/1342.pdf

Ulff-Moller, F., Choi, B.-G., Rubin, A.E., Tran, J., Wasson, J.T. (1998) Meteorit Planetary Scien - 2010 - ULFF-MØLLER - Paucity of sulfide in a large slab of Esquel New perspectives on.pdf. *Meteoritics & Planetary Science* 33, 221–227. https://doi.org/10.1111/j.1945-5100.1998.tb01627.x

Van Roosbroek, N. et al. (2015) The formation of IIE iron meteorites investigated by the chondrule - bearing Mont Dieu meteorite. *Meteoritics & Planetary Science* 50, 1173–1196. https://doi.org/10.1111/maps.12463

Wang, P.-L., Rumble, D., McCoy, T.J. (2004) Oxygen isotopic compositions of IVA iron meteorites: implications for the thermal evolution derived from in situ ultraviolet laser microprobe analyses. *Geochimica et Cosmochimica Acta* 68, 1159–1171. https://doi.org/10.1016/j.gca.2003.08.016

Wasson, J.T. (1969) The chemical classification of iron meteorites-III. Hexahedrites and other irons with germanium concentrations between 80 and 200 ppm. *Geochimica et Cosmochimica Acta* 33, 859–876. https://doi.org/10.1016/0016-7037(69)90032-5

Wasson, J.T. (1999) Trapped melt in IIIAB irons; solid/liquid elemental partitioning during the fractionation of the IIIAB magma. *Geochimica et Cosmochimica Acta* 63, 2875–2889. https://doi.org/10.1016/S0016-7037(99)00283-5

Wasson, J.T., Kimberlin, J. (1967) The chemical classification of iron meteorites—II. Irons and pallasites with germanium concentrations between 8 and 100 ppm. *Geochimica et Cosmochimica Acta* 31, 2065–2093. https://doi.org/10.1016/0016-7037(67)90143-3

Wasson, J.T., Sedwick, S.P. (1969) Possible Sources of Meteoritic Material from Hopewell Indian Burial Mounds. *Nature* 222, 22–24. https://doi.org/10.1038/222022a0

Wasson, J.T., Wang, J. (1986) A nonmagmatic origin of group-IIE iron meteorites. *Geochimica et Cosmochimica Acta* 50, 725–732. https://doi.org/10.1016/0016-7037(86)90348-0

Wasson, J.T., Choi, B.-G., Jerde, E.A., Ulff-Møller, F. (1998) Chemical Classification of Iron Meteorites: XII. New Members of the Magmatic Groups. *Geochimica et Cosmochimica Acta* 62, 715–724. https://doi.org/10.1016/S0016-7037(97)00379-7

Wasson, J.T., De Bon, C.C. (1998) New Chilean iron meteorites: Medium octahedrites from Northern Chile are unique. *Meteoritics & Planetary Science* 33, 175–179. https://doi.org/10.1111/j.1945-5100.1998.tb01623.x

Wasson, J.T., Kallemeyn, G.W. (2002) the IAB iron-meteorite complex: A group, five subgroups, numerous grouplets, closely related, mainly formed by crystal segregation in rapidly cooling melts. *Geochimica et Cosmochimica Acta* 66, 2445–2473. https://doi.org/10.1016/S0016-7037(02)00848-7

Wasson, J.T., Choi, B.-G. (2003) Main-group pallasites: Chemical composition, relationship to IIIAB irons, and origin. *Geochimica et Cosmochimica Acta* 67, 79–3096. https://doi.org/10.1016/S0016-7037(03)00306-5

Wieler, R. (2002) Cosmic-Ray-Produced Noble Gases in Meteorites. *Reviews in Mineralogy and Geochemistry* 47, 125–170. https://doi.org/10.2138/rmg.2002.47.5

Windmill, R.J., Franchi, I.A., Hellmann, J.L., Schneider, J.M., Spitzer, F., Kleine, T., Greenwood, R.C., Anand, M. (2022) Isotopic evidence for pallasite formation by impact mixing of olivine and metal during the first 10 million years of the Solar System. *PNAS Nexus* 1, pgac015. https://doi.org/10.1093/pnasnexus/pgac015

Worsham, E.A., Burkhardt, C., Budde, G., Fischer-Gödde, M., Kruijer, T.S., Kleine, T. (2019) Distinct evolution of the carbonaceous and non-carbonaceous reservoirs: Insights from Ru, Mo, and W isotopes. *Earth and Planetary Science Letters* 521, 103–112. https://doi.org/10.1016/j.epsl.2019.06.001

Wood, B.J., Smythe, D.J., Harrison, T. (2019) The condensation temperatures of the elements: A reappraisal. *American Mineralogist*, *104*(6), 844-856. https://doi.org/10.2138/am-2019-6852CCBY

Yokoyama, T., Nagai, Y., Fukai, R., Hirata, T. (2019) Origin and Evolution of Distinct Molybdenum Isotopic Variabilities within Carbonaceous and Noncarbonaceous Reservoirs. *The Astrophysical Journal* 883, 62. https://doi.org/10.3847/1538-4357/ab39e7

Zimmermann, L., Füri, E., Boulliung, J., Saxton, J.M. (2025) Performance of the 3F4M Noblesse–HR Noble Gas Mass Spectrometer for Multicollection Ne - Ar - N2 Analyses. *Geochemistry, Geophysics, Geosystems* 26. https://doi.org/10.1029/2025GC012247